ISSN (Print) 1226-1750
ISSN (Online) 2233-6656
Journal of Magnetics 27(4), 474-479 (2022) https://doi.org/10.4283/JMAG.2022.27.4.474

Design of a Depth-Encoding Detector for PET Through Insertion of Light Guide Between Crystal Arrays

Seung-Jae Lee[1] and Cheol-Ha Baek[2]*

[1]Department of Radiological Science, Dongseo University, Busan 47011, Korea
Center for Radiological Environment & Health Science, Dongseo University, Busan 47011, Korea
[2]Department of Radiological Science, Kangwon National University, Samcheok 25949, Korea
Department of Medical Health Science, Kangwon National University, Samcheok 25949, Korea

(Received 28 September 2022, Received in final form 19 December 2022, Accepted 20 December 2022)

To improve the spatial resolution of preclinical positron emission tomography (PET), a detector consisting of a two-layer scintillator pixel array was designed. A light guide was inserted between the arrays of scintillators to change the distribution of light generated in each layer. By analyzing the different light distributions, it is possible to track where the gamma rays interacted. To this end, a gamma ray event was generated at the center of the flashing pixel and a lookup table was created based on the signal obtained from the light sensor. The optimal position of the scintillation pixel was tracked through comparison and analysis of the newly detected signal with the look-up table through maximum likelihood position estimation. As a result, excellent accuracy was shown. If this detector is used in a preclinical PET system, it is expected to show excellent spatial resolution, and since an optical sensor that is not affected by magnetic fields is used, it is considered that it can be applied to PET/MRI in the future.

Keywords : detector, light distribution, light guide, simulation, MLPE, PET/MRI

1. Introduction

Preclinical Positron Emission Tomography (PET) requires higher spatial resolution to image small animals. There are several ways to achieve better spatial resolution: making the area of the crystal pixel where gamma rays are incident small; using a small gantry to increase the sensitivity; using long crystal pixels [1]. In other words, small and long crystals are necessary to achieve good spatial resolution and sensitivity. When applying small and long crystal pixels to a detector and configuring a PET system, spatial resolution degrades at the outer area of the field of view (FOV) [2, 3]. In a PET system, all detectors are arranged to face the center of the FOV. Therefore, gamma rays generated from the center of the FOV are incident perpendicularly to the detectors, whereas gamma rays generated outside the FOV are incident obliquely to the crystal pixels (Fig. 1). Because the energy of gamma rays generated outside the FOV is high, gamma rays are detected over several crystals. When reconstructing the detected gamma rays generated from the center of the FOV, there is no degradation in spatial resolution, as all gamma rays are vertically incident on crystals and detected only in one crystal pixel. However, the spatial resolution reduces when reconstructing gamma rays generated outside the FOV because the gamma rays are detected from several crystals. Many studies have tried to develop detectors that measure the depth position where gamma-ray and crystal interact to solve the degradation of spatial resolution outside the FOV. The developed detectors are classified as follows: (1) Arranging crystal pixels in multiple layers [4-10], (2) Using a single-layer crystal pixel array and placing optical sensors on both sides [11-13], and (3) Using block-type scintillators and measuring changes in the signals by heights [14, 15]. These detectors go through a few steps to find the locations of the crystal pixels that interact with gamma rays: reconstructing flood images based on the signals obtained from the detector and dividing the areas in the flood images where each crystal pixel is recorded. In short, the locations of the crystal pixels are determined by acquiring signals from the

*Corresponding author: Tel: +82-33-540-3384
Fax: +82-33-540-3389, e-mail: baekch@kangwon.ac.kr

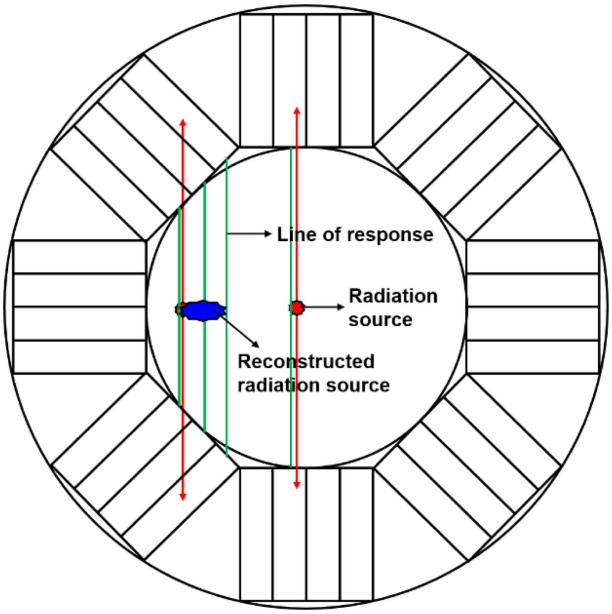

Fig. 1. (Color online) Schematic diagram indicating the degradation of spatial resolution in the peripheral of the FOV. If the radiation source is the peripheral of the FOV, it can be detected in several scintillation pixels, so spatial resolution is reduced when reconstructed into an image. The red lines indicate the generated directions of the radiation source, and the green lines are the lines of responses between the detected crystal pixels.

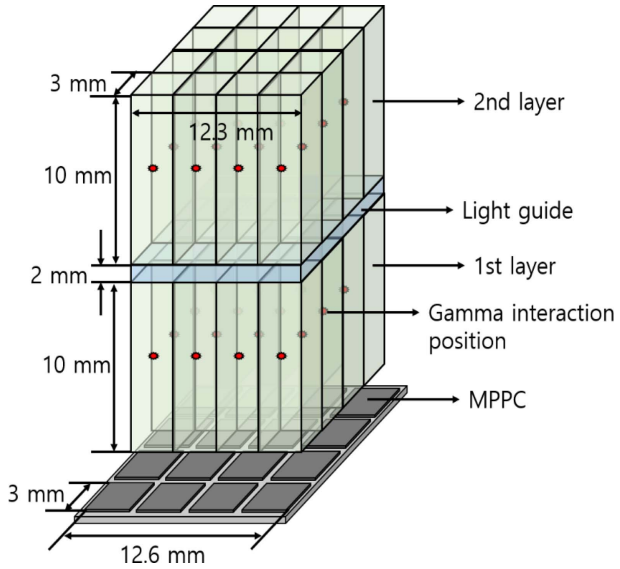

Fig. 2. (Color online) Schematic diagram of a detector with two layers of crystal pixels in 4 × 4 arrays. A light guide is inserted between the layers, and the light generated by interaction with gamma rays is detected by MPPCs. By inserting the light guide between the layers, the distribution of the light generated from the scintillation pixels is changed.

photosensors, processing reconstructing flood images, and dividing regions.

We developed a detector that directly tracks the locations where gamma rays and crystal pixels interact in three dimensions through the MLPE(the maximum likelihood position estimation) method [16] instead of a region segmentation method that requires several signal processes. This detector consists of two layers with a light guide inserted between the layers, so it distinguishes layers by differentiating the light distribution of each layer generated from the interactions of crystal pixels and gamma rays. For designing the detector, DETECT2000, which can simulate the light of a detector with scintillators and optical sensors, analyzed the characteristics [17, 18].

2. Materials and Methods

2.1. Detector design

We designed a detector using DETECT2000, which can simulate the light in a detector. The simulation tool, DETECT2000, simulates the movement, scattering, absorption, and reflection of light generated by the interaction between gamma rays and scintillators. It also measures the number of incident lights through optical sensors. The type of material used in the simulation can be expressed as a refractive index. It is possible to change the light distribution and measurement rate in the optical sensor according to the light reflection by using a reflectance applied to a reflector as an input variable. Accordingly, a detector was designed as shown in Fig. 2. This dual-layer detector consists of crystals with dimensions of 3 mm × 3 mm × 10 mm in a 4 × 4 array for each layer. We inserted a light guide between the layers so that the light distribution of each layer was measured differently by the photosensors. Because the light distribution measured by photosensors differs from layer to layer, the MLPE method can distinguish each layer. As for the crystal pixel used, a GAGG ($Gd_3Al_2Ga_3O_{12}$) scintillator was used, which has an excellent gamma-ray detection rate due to its high light output of 50,000 photons/MeV and a high density of 6.6 g/cm3 [19]. The refractive index of GAGG is 1.91, and the peak emission wavelength is 530 nm. The light guide is made of K-9 glass material, has dimensions of 12.3 mm × 12.3 mm × 2 mm, and has a refractive index of 1.51630 [20]. A reflector was used between crystals to let the light generated from interaction with gamma rays move to the photosensor as much as possible. 3M's Enhanced Specular Reflector (ESR) was simulated as a reflector, and the reflectance was set to 98 % [21]. For optical sensors, the model s14161-3050HS-04, multi-

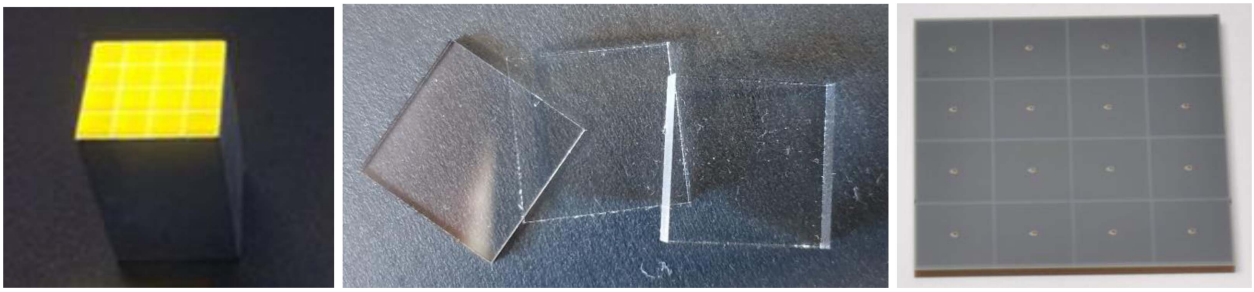

Fig. 3. (Color online) Examples of GAGG scintillators, light guides and MPPCs used to configure the detector. The light guide is transparent glass and changes the distribution of light generated from the scintillator. Left: GAGG scintillators, Center: Light guides, Right: MPPCs.

pixel Photon Counters (MPPCs) from Hamamatsu, was simulated to measure generated light [22]. MPPCs are compact silicon photomultipliers, so the overall size of a detector can be made small. They are also used in a magnetic field because they're not affected by magnetic fields. The size of the MPPCs is 12.6 mm × 12.6 mm, and it consists of MPPC pixels size of 3 mm × 3 mm in a 4 × 4 array with a distance of 0.2 mm between each pixel. Fig. 3 shows examples of GAGG scintillators, light guides, and MPPCs. Optical grease (refractive index: 1.465) was used between crystal pixels, the light guide, and the photosensors to minimize light loss resulting from light refraction and total reflection of light due to sharp differences in the refractive indexes.

2.2. Creating look-up tables

We created lookup tables for each crystal pixel to apply the MLPE method. The gamma-ray events were generated at the center of each crystal, and the light was collected from each optical sensor to create lookup tables. For the number of generated light, 511 keV, which is the energy of extinction radiation, the amount of light generated according to the radiation energy of the GAGG scintillator, and the light detection efficiency of MPPC according to the wavelength of light were applied. 16 MPPCs collected the light generated by the gamma-ray events at the centers of all crystals. As shown in Fig. 4, 16 collected data were processed with 4 channels each on the x and y-axis, a total of 8 channels. Reducing the data channels make the configuration of the electronic circuit simplified. After calculating the average value and standard deviation value of the data of each channel, lookup tables were created accordingly. The three-dimensional position of the crystal pixel interacting with gamma rays was measured by the created lookup tables also by calculating the collected data from the new gamma-ray events using the following equation.

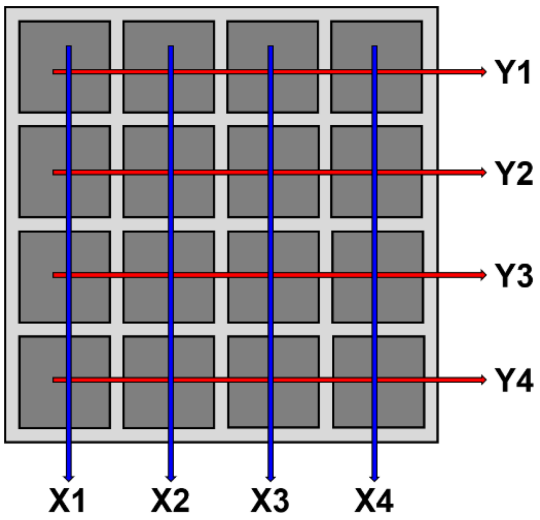

Fig. 4. (Color online) The data acquired from 16 MPPCs was reduced to 4 channels each on the x and y-axis, a total of 8 channels. Signals for each of the four photosensor pixels were summed in the x and y-axis, respectively.

$$\ln \Pr[M_i|x] = -\left(\sum_{i=1}^{n} \frac{(M_i - \mu(x))^2}{2\sigma_i^2(x)} + \sum_{i=1}^{n} \ln \sigma_i(x) \right)$$

In this equation, M represents the signals of 8 channels acquired from gamma-ray events of each location of crystals. μ and σ represent the average and standard deviation values for each location of crystals in the lookup tables, respectively.

2.3. Accuracy evaluation of measured locations by gamma-ray events

We generated gamma-ray events in the depth direction of all crystals to evaluate the accuracy of locations of crystals; the locations where crystals interact with newly incident gamma-rays and induced by lookup tables,

MLPE method, and detectors composed of two layers of crystals. 100 gamma rays events occurred at the centers of crystal pixels for the x and y-axis. For the z-axis (depth) direction, we generated 100 gamma-ray events at each location with an interval of 0.2 mm from 0.1 mm to 9.9 mm in the lower layer and from 12.3 mm to 22.1 mm in the upper layer. Each MPPC detected the light generated by gamma-ray events in the depth direction, and the optimal position of crystal was measured through MLPE by reducing the data into 8 channels. We evaluated the accuracy by comparing the measured locations with the locations where the gamma-ray events were generated.

3. Results

We constructed a two-layer detector consisting of GAGG crystals in 4 × 4 arrays, a light guide, and MPPCs. Fig. 5 shows a flood image acquired by general image processing processed by the proposed detector. Each layer is distinguishable at the peripheral crystals, but all center crystals overlap. In other words, the region division of the flood image doesn't make it possible to distinguish the layers where the scintillator and the gamma-ray interact. However, when using the MLPE method according to the light distribution, the layers are distinguished as the light distribution of each layer is different. By inserting a light guide between the arrays of crystals, light distributions detected by MPPCs become different for each layer.

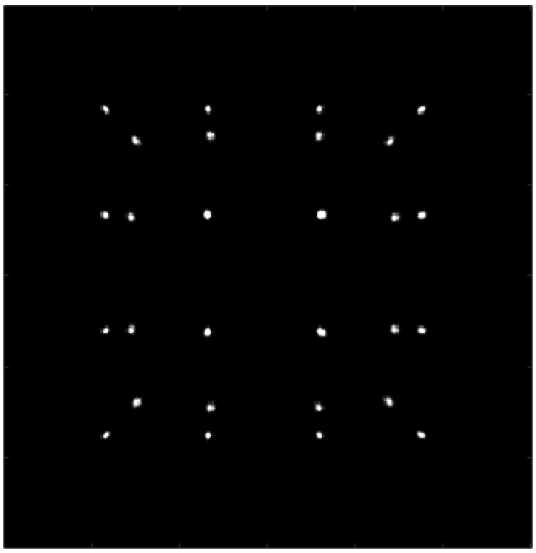

Fig. 5. (Color online) A flood image is acquired through a general image processing process. The edge and corner crystals can be distinguished by layer, but all the crystals in the center overlap, making it impossible to distinguish between layers.

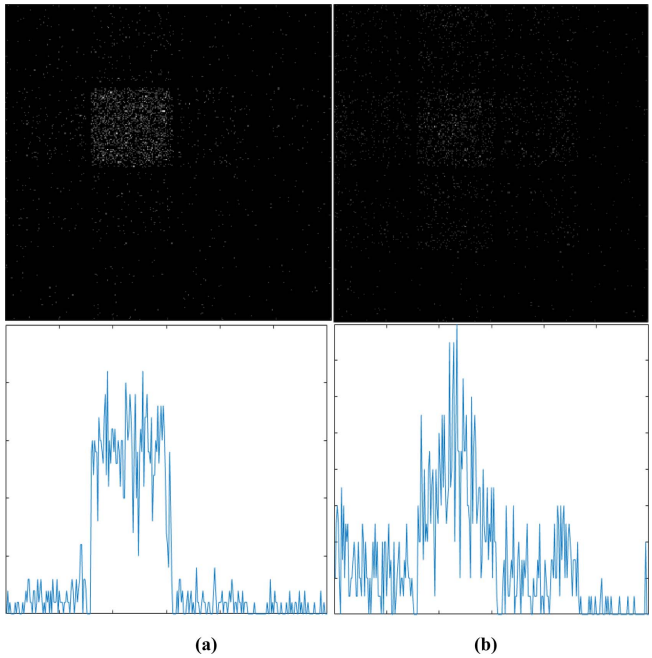

Fig. 6. (Color online) Distribution in MPPCs of light generated at coordinates (2, 2) of crystal pixel position for each layer. It can be seen that the light is distributed more at the corresponding crystal pixel location in the first layer than in the second layer.

Fig. 6(a) shows the light distribution and the profile measured in MPPCs when generating gamma events at the coordinates of the crystal pixel position (2, 2), the center of an upper layer. Fig. 6(b) shows the light distribution and the profile of a lower layer. The light

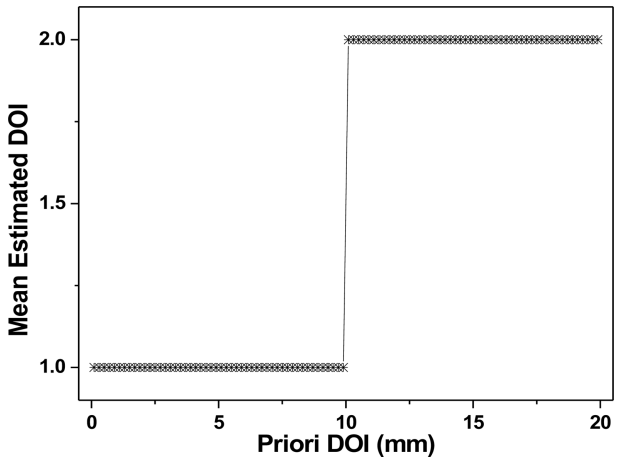

Fig. 7. Depth of interaction (DOI) position results of each layer. The horizontal axis represents the simulation position, and the vertical axis represents the measured average position along with the simulation position. It can be seen that the layer division is perfectly separated at 10 mm.

distribution was measured more at the positions of crystal pixels in the first layer than the second layer, as profiles verify clearly. The light distribution of the first layer showed a significantly higher value at the positions of crystal pixels than at the other positions, while the light distribution of the second layer was distributed more widely than that of the first layer.

Accuracy measurements for coordinates and depth directions of crystal pixels through MLPE showed excellent results. The measurement results of the x and y-axis and the depth direction were all excellent. Fig. 7 shows the degree of layer distinction according to the depths at which gamma-ray events were generated. The thickness of the light guide is not indicated on the graph but shown only as values corresponding to the lengths of the crystal pixels. In other words, 0.1-9.9 mm and 10.1-19.9 mm represent the first and second layers, respectively. The distinction of the layers occurred at 9.9 mm and 10.1 mm.

4 Discussion and Conclusions

We designed a detector that measures the locations of crystal pixels interacting with gamma rays. This detector consists of two layers of crystal pixels, with a light guide inserted between the layers. Light generated from the upper and lower layers is detected with different distributions in the MPPCs due to the light guide inserted between the layers. Accordingly, we created lookup tables for the distribution of each layer and measured the three-dimensional positions of crystal pixels interacting with gamma rays through the MLPE method. All the measurement results showed excellent accuracy not only for the x and y-axis but also for the z-axis. This result seems to come out because of designing the detector through simulation and creating lookup tables under perfect conditions. However, the positions were the center of crystals when creating lookup tables for the depth direction, while data for evaluating the accuracy of the depth direction was acquired from all positions of crystals. The distributions obtained by depth were slightly different, but the results of layer measurement using the MLPE method showed perfect accuracy. It indicates that even if there is a certain degree of change in the distributions, the MLPE method still has excellent measurement ability when measuring the layers.

In future research, we intend to experimentally measure and analyze the three-dimensional position by constructing a detector based on the simulation results. If we use the proposed detector of this study, the detector will resolve the degradation of spatial resolution in the peripheral of the FOV in preclinical PET. In addition, a three-dimensional position can be obtained directly as a coordinate value of a crystal, away from the method of distinguishing layers by separating the regions of each crystal pixel after acquiring a flood mage. Since an optical sensor that is not affected by magnetic fields is used, it is considered that it can be applied to PET/MRI in the future.

Acknowledgments

This work was supported by Dongseo University, “Dongseo Cluster Project” Research Fund of 2022 (DSU-20220004).

References

[1] F. Habte, A. M. K. Foudray, P. D. Olcott, and C. S. Levin, Phys. Med. Biol. **52**, 3753 (2007).
[2] R. S. Miyaoka, T. K. Lewellen, H. Yu, and D. L. McDaniel, IEEE Tran. Nucl. Sci. **45**, 1069 (1998).
[3] L. R. MacDonald, M. Dahlbom, Levin, IEEE Tran. Nucl. Sci., **45**, 2232 (1998).
[4] J. H. Jung, Y. Choi, Y. H. Chung, O. Devpoede, M. Krieguer, P. Bruyndonckx, and S. Tavernier, Nucl. Inst. Meth. A **571**, 669 (2007).
[5] M. Ito, J. S. Lee, S. I. Kwon, G. S. Lee, B. Hong, K. S. Lee, K. S. Sim, S. J. Lee, J. T. Rhee, and S. J. Hong, IEEE Tran. Nucl. Sci. **57**, 976 (2010).
[6] H. Murayama, I. Ishibashi, H. Uchida, T. Omura, and T. Yamashita, IEEE Tran. Nucl. Sci. **45**, 1152 (1998).
[7] T. Tsuda, H. Murayama, K. Kitamura, T. Yamaya, E. Yoshida, T. Omura, H. Kawai, N. Inadama, and N. Orita, IEEE Tran. Nucl. Sci. **51**, 2537 (2004).
[8] S.-J. Lee and C-H. Baek, Nucl. Inst. Meth. A **887**, 13 (2018).
[9] C. S. Levin, IEEE Tran. Nucl. Sci. **49**, 2236 (2000).
[10] A. Vandenbroucke, A. M. K. Foudray, P. D. Olcott, and C. S. Levin, Phys. Med. Biol. **55**, 5895 (2010).
[11] Y. Shao, R. W. Silverman, R. Farrell, L. Cirignano, R. Grazioso, K. S. Shah, G. Visser, M. Clajus, T. O. Tumer, and S. R. Cherry, IEEE Tran. Nucl. Sci. **47**, 1051 (2000).
[12] Y. Yang, J. Qi, Y. Wu, S. S. James, R. Farrell, P. A. Dokhale, K. S. Shah, and S. R. Cherry, Phys. Med. Biol. **54**, 433 (2009).
[13] H. Du, Y. Yang, and S. R. Cherry, Phys. Med. Biol. **52**, 2499 (2007).
[14] Y. H. Chung, C-H. Baek, S-J. Lee, K. J. Hong, J. H. Kang, and Y. Choi, Nucl. Inst. Meth. A **621**, 590 (2010).
[15] S-J. Lee, C-H. Baek, and Y. H. Chung, Jour. Kor. Phys. Soc. **54**, 2429 (2009).
[16] H. H. Barrett, W. C. J. Hunter, B. W. Miller, S. K. Moore, Y. Chen, and L. R. Furenlid, IEEE Tran. Nucl. Sci. **56**,

725 (2009).
[17] F. Cayouette, D. Laurendeau, C. Moisan, Proceedings of SPIE, Quebec, **4833**, 69 (2003).
[18] F. Cayouette, C. Moisan, N. Zhang, and C. J. Thompson, IEEE Tran. Nucl. Sci. **49**, 624 (2002).
[19] https://www.epic-crystal.com/matrix-and-arrays/gagg-ce-array.html
[20] https://www.epic-crystal.com/others/light-guide.html
[21] https://multimedia.3m.com/mws/media/1389248O/application-guide-for-esr.pdf
[22] https://www.hamamatsu.com/content/dam/hamamatsu-photonics/sites/documents/99_SALES_LIBRARY/ssd/s14160_s14161_series_kapd1064e.pdf